Analysis of Nonlinear Panel Flutter and Response under Random Excitation or Nonlinear Aerodynamic Loading

FRANKLIN E. EASTEP*
Air Force Institute of Technology, Wright-Patterson Air Force Base, Ohio
AND
SAMUEL C. MCINTOSH JR.†
Stanford University, Stanford, Calif.

Since the exact solution to von Kármán's large deflection equations is unknown, the Rayleigh-Ritz approximation to Hamilton's variational principle is used to investigate nonlinear panel flutter. Solution to this problem is given for 1) random excitation and linear aerodynamic loading, and 2) nonlinear aerodynamic loading alone. For 1, the limit-cycle oscillation is determined by representing the modal amplitudes by a Fourier series and applying the Galerkin averaging for the temporal solution. The existence of a limit cycle is determined by investigating the stability of small perturbations about the limit cycle solution. Random excitation provided by a known pressure with spatial and temporal random variation is introduced and treated. For 2, a two-dimensional panel with aerodynamic loads obtained from nonlinear piston theory is examined. A coupled set of quasi-linear second order differential equations in time is derived for the modal amplitude. These equations are then integrated from given initial conditions to provide the panel motion versus time. The importance of various nonlinear aerodynamic terms is assessed and the implication of the significant terms with respect to panel stability and postcritical response is discussed.

Nomenclature

A = aerodynamic pressure, lb/in.^{2}
B_m = modal amplitudes for in-plane displacement
C_n = modal amplitude of panel oscillation
C_{ni} = harmonic of modal amplitude
$\mathbf{C}_0$ = state-space vector of initial values for modal amplitudes and velocities
D = flexural stiffness $D = Eh^3/12(1 - \nu^2)$(in.-lb)
E = Young's modulus, lb/in.^{2}
E_0 = total energy
F = Airy stress function, lb
K = running spring constant for in-plane restraint spring
M = airstream Mach number
$\bar{N}_x$ = applied longitudinal axial load, lb/in.
N_y = applied spanwise load, lb/in.
U_∞ = speed of airstream, mph
a = plate length, in.
b = plate width, in.
h = panel thickness, in.
p = applied pressure, lb/in.^{2}
p_s = static pressure, lb/in.^{2}
p_{nR} = modal random pressure, lb/in.^{2}
q = airstream dynamic pressure $q = \frac{1}{2}\rho_\infty U_\infty^2$, lb/in.^{2}
t = time variable, sec
α = longitudinal wave length for plate $\alpha = \pi/a$
α' = in-plane restraint parameter
β_A = $(M^2 - 1)^{1/2}$ compressibility correction factor
γ = aerodynamic mass ratio
γ_a = gas constant for air ($\gamma_a = 1.4$)
ϵ_F = limit cycle modal phase difference
κ = damping parameter $\kappa = (\gamma\lambda/M)^{1/2}$
λ = dynamic pressure parameter, lb/in.^{2}
μ = deformation aspect ratio for a plate $\mu = ja/b$
ρ = panel density, lb/in.^{3}
ρ_∞ = airstream density, lb/in.^{3}
σ_{xm} = midsurface extensional stress in longitudinal direction, lb/in.^{2}
σ_{ym} = midsurface extensional stress in spanwise direction, lb/in.^{2}
τ_{xym} = midsurface shearing strain
τ = time variable, sec
ν = Poisson ratio
ω = frequency of oscillation, rad/sec

Received June 8, 1970; revision received July 30, 1970. Research supported in part by NASA Grant NGR 05-020-102.

* Assistant Professor, Department of Mechanics. Member AIAA.
† Acting Assistant Professor, Department of Aeronautics and Astronautics. Member AIAA.

I. Introduction

PANEL flutter differs from wing flutter in two significant ways: 1) the airflow is only on one side of the panel, and 2) the nature of the panel flutter is generally not as catastrophic as wing flutter. As predicted by linear theory the amplitude of response to any initial disturbance rapidly decays, but on the unstable side the amplitude of oscillation increases without bound. In actual practice, panel flutter is characterized by the fact that the amplitude of panel oscillation is limited by the nonlinear interaction of in-plane stresses and transverse deformation. This suggests that skin panels could safely exist for long periods of exposure to conditions beyond the linear flutter boundaries. Accordingly, the theoretical problem of predicting the response (and ultimately the stresses) in nonlinear aeroelastic systems is receiving increased attention with the aim of developing criteria for a fatigue-based structural synthesis.

At the present time there is still in many cases poor correlation between experimental and theoretical flutter prediction. Where it is in error the theoretical prediction of panel flutter has been overly conservative. This fact is demonstrated by flight vehicles that have flown successfully with skin thicknesses smaller than those recommended for flutter safety. Because of the complexity of panel flutter, most theoretical studies make use of simplifying assumptions. However, these assumptions are usually so restrictive that the theoretical model does not accurately represent realistic conditions. The disagreement between theoretical and experimental flutter prediction can be attributed in part to the following: 1) imprecise idealization of all the complicated panel support conditions that can occur (the neglect of nonlinear midplane tensile stresses is assumed to be the major result of this over-

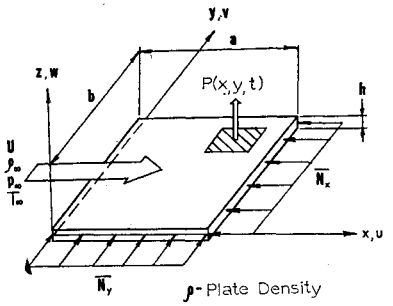

Fig. 1 A thin elastic plate simply supported on four edges.

idealization); 2) neglect of boundary-layer effects, particularly panel excitation by turbulence; and 3) use of a linear aerodynamic theory.

II. Equations for Panel Oscillation

Consider the isotropic, thin-walled plate shown in Fig. 1. It is exposed to a supersonic airstream on one side only and also subjected to longitudinal and spanwise axial loads, a static pressure difference, and a transverse random pressure of known spatial and temporal distribution. It is assumed that the large oscillations of the plate in the presence of midsurface forces are governed by von Karman's large deflection equations.[1] These equations are

$$D\nabla^4 w - h\left(\frac{\partial^2 F}{\partial y^2}\frac{\partial^2 w}{\partial x^2} - 2\frac{\partial^2 F}{\partial x \partial y}\frac{\partial^2 w}{\partial x \partial y} + \frac{\partial^2 F}{\partial x^2}\frac{\partial^2 w}{\partial y^2}\right) + \bar{N}_x\frac{\partial^2 w}{\partial x^2} + \bar{N}_y\frac{\partial^2 w}{\partial y^2} = p_R(x,y,t) + A - \rho h\frac{\partial^2 w}{\partial t^2} + p_s \quad (1)$$

and

$$\nabla^4 F = E[(\partial^2 w/\partial x \partial y)^2 - (\partial^2 w/\partial x^2)\partial^2 w/\partial y^2] \quad (2)$$

where w is the panel deflection and p_R is a transverse random pressure. The aerodynamic pressure loading A, resulting from plate deformation, will be assumed to be given by linear piston theory.

$$A = (2q/\beta_A)[\partial w/\partial x + (M^2 - 2)/(M^2 - 1)(1/U_\infty)\partial w/\partial t] \quad (3)$$

Generally, nonlinear panel flutter is investigated by solving Eqs. (1, 2, and 3) with Galerkin's method. Although Galerkin's method is one of the most widely used approximate methods for panel flutter prediction, there are some doubts about the applicability of the method with all the complex boundary conditions that can occur in practice. It therefore appears advisable to investigate the panel flutter problem with a true variational principle. The Rayleigh-Ritz approximation to Hamilton's variational principle will be employed to accomplish this reinvestigation. The assumed transverse deformation is given by

$$w(x,y,t) = \sum_{m=1}^{M}\sum_{n=1}^{N} C_{nm}(t)\varphi_n(y)\varphi_m(x) \quad (4)$$

where M and N are chosen large enough to adequately represent the deformation, w. A two mode approximation for a simply supported plate is

$$w(x,y,t) = h[C_1(t)\sin(\pi x/a) + C_2(t)\sin(2\pi x/a)]\sin(j\pi y/b) \quad (5)$$

where j identifies the spanwise mode. This two mode approximation is not accurate enough to insure quantitative convergence of solutions but promotes computation ease and demonstrates the general method. The inclusion of more modes will be accomplished in a later section of this paper.

Substituting Eq. (5) into Eq. (2) yields a partial differential equation from which the stress function F can be determined as

$$F = -\bar{N}_x y^2 - \bar{N}_y x^2 + Eh^2\mu^2\left\{-\frac{C_1C_2}{4}\cos\alpha x + \frac{C_1^2}{32}\cos 2\alpha x + \frac{C_1C_2}{36}\cos 3\alpha x + \frac{C_2^2}{128}\cos 4\alpha x + \left[\frac{C_1^2 + 4C_2^2}{32\mu^4} + \frac{9C_1C_2}{4(1+4\mu^2)^2}\cos\alpha x - \frac{C_1C_2}{4(9+4\mu^2)^2}\cos 3\alpha x\right]\cos\frac{2j\pi y}{b}\right\} \quad (6)$$

Now the midplane stresses resulting from large oscillation of the plate can be determined from the definition of the Airy stress function. With midplane tensile stresses thus determined it is possible to use Hamilton's variational principle to obtain the transverse equation of plate motion rather than solving Eq. (1) with the aid of Galerkin's averaging method. Hamilton's principle is given as

$$\delta\int_{t_1}^{t_2}(T - U - V)dt + \int_{t_1}^{t_2}\delta W_e dt = 0 \quad (7)$$

where δ indicates admissible variations in the degrees of freedom characterizing the state of deformation. T is the kinetic energy, U is the strain energy, V is the potential of all applied conservative loads and δW_e is virtual work of all unconservative loads.

The strain energy due to both midplane stresses and bending stresses is

$$U = \frac{h}{2E}\int_0^a\int_0^b[(\sigma_{xm} + \sigma_{ym})^2 - 2(1+\nu)\times(\sigma_{xm}\sigma_{ym} - \tau_{xym}^2)]dxdy + \frac{D}{2}\int_0^a\int_0^b\left[\left(\frac{\partial^2 w}{\partial x^2}\right)^2 + \left(\frac{\partial^2 w}{\partial y^2}\right)^2 + 2\nu\frac{\partial^2 w}{\partial x^2}\frac{\partial^2 w}{\partial y^2} + 2(1-\nu)\left(\frac{\partial^2 w}{\partial x \partial y}\right)^2\right]dxdy \quad (8)$$

The transverse kinetic energy due to a plate oscillation is

$$T = \frac{\rho h}{2}\int_0^a\int_0^b\left(\frac{\partial w}{\partial t}\right)^2 dxdy \quad (9)$$

The potential energy of the applied conservative loads (due to applied midplane forces, static pressure differential and random pressures) is

$$V = \bar{N}_x\int_0^a\int_0^b\left[\frac{\sigma_{xm} - \nu\sigma_{ym}}{E} - \frac{1}{2}\left(\frac{\partial w}{\partial x}\right)^2\right]dxdy + \bar{N}_y\int_0^a\int_0^b\left[\frac{\sigma_{ym} - \nu\sigma_{xm}}{E} - \frac{1}{2}\left(\frac{\partial w}{\partial y}\right)^2\right]dxdy + p_s\int_0^a\int_0^b w dxdy + \int_0^a\int_0^b p_R(x,y,t)w dxdy \quad (10)$$

The virtual work of the applied nonconservative forces (aerodynamic pressure induced by plate deformation) can be determined for each of the virtual displacements δC_1 and δC_2

$$\delta W_{ec1} = \int_0^a\int_0^b Ah\sin\alpha x\sin\frac{j\pi y}{b}\delta C_1 dxdy \quad (11)$$

$$\delta W_{ec2} = \int_0^a\int_0^b Ah\sin 2\alpha x\sin\frac{j\pi y}{b}\delta C_2 dxdy \quad (12)$$

Hamilton's variational principle is satisfied with respect to the degrees of freedom $C_1(t)$ and $C_2(t)$. The resulting equations of motion are

$$\frac{d^2C_1}{d\tau^2} + \left(\frac{\gamma\lambda}{M}\right)^{1/2}\frac{dC_1}{d\tau} + (M_1 + N_1C_1^2 + QC_2^2)C_1 - \frac{8\lambda}{3}C_2 = \frac{8}{j\pi^2}[1 - (-1)^j]p_s + p_{1R} \quad (13)$$

$$\frac{d^2C_2}{d\tau^2} + \left(\frac{\gamma\lambda}{M}\right)^{1/2}\frac{dC_2}{d\tau} + (M_2 + N_2C_2^2 + QC_1^2)C_2 + \frac{8\lambda}{3}C_1 = p_{2R} \quad (14)$$

where

$$\tau = \left(\frac{D}{\rho h}\right)^{1/2}\alpha^2 t; \quad N_x = \frac{\bar{N}_x}{D\alpha^2}; \quad N_y = \frac{\bar{N}_y}{D\alpha^2}; \quad \gamma = \frac{\rho_\infty a}{\rho h};$$

$$\lambda = \frac{2qa^3}{\pi^4\beta D}; \quad p_s = \frac{p_s\alpha^4}{Dh}$$

$$p_{1R} = \frac{4\alpha^4}{Dh^2ab}\int_0^a\int_0^b p_R\frac{\partial w}{\partial C_1}\,dxdy;$$

$$p_{2R} = \frac{4\alpha^4}{Dh^2ab}\int_0^a\int_0^b p_R\frac{\partial w}{\partial C_2}\,dxdy$$

$$M_1 = (1+\mu^2)^2 - (N_x + \mu^2 N_y); \quad M_2 = (4+\mu^2)^2 - (4N_x + \mu^2 N_y)$$

$$N_1 = 12(1-\nu^2)(1+\mu^4)/16; \quad N_2 = 12(1-\nu^2)(16+\mu^4)/16$$

$$Q = 12(1-\nu^2)[(1+\mu^4)/4 + 8\mu^4/16(1+4\mu^2)^2 + \mu^4/16(9+4\mu^2)]$$

III. Determination of Limit-Cycle Oscillation

Equations (13) and (14) represent a coupled set of second-order, nonlinear, ordinary differential equations for the determination of the time history of the modal amplitudes. With these equations the nature of the plate motion can be studied for different values of dynamic pressure, Mach number, structural damping, static pressure, random pressure and applied midplane forces. An approximate technique will be used to solve Eqs. (13) and (14). This technique was first used by Küssner[2] in his study of nonlinear wing flutter.

Temporarily, the effect of the random pressure resulting from the turbulent boundary layer over the plate will be neglected. Experiments have shown that the flutter motion of flat plates above the linear stability boundary is a limit-cycle oscillation. It will therefore be assumed that each of the modal amplitudes can be represented as a finite Fourier series

$$C_n(\tau) = \sum_{r=-N}^{N} C_{nr}e^{ir\omega\tau} \qquad n = 1,2 \quad (15)$$

It should be noted that $C_{n(-r)} = C_{nr}^*$, the conjugate complex of C_{nr}.

Equation (15) is substituted into Eqs. (13) and (14), which results in two nonlinear algebraic equations, $NL_m = 0$; $m = 1,2$. The Galerkin averaging technique is then applied to these two nonlinear equations over one period of oscillation.

$$\int_0^{2\pi/\omega} NL_m(C_{1r},C_{2r},\omega)\frac{\partial C_n}{\partial C_{nr}}\,d\tau = 0 \qquad m,n,r = 1,2 \quad (16)$$

This procedure yields the following system of nonlinear algebraic equations:

$$[-r^2\omega^2 + \kappa ir\omega + M_1]C_{1r} + \sum_{s=-N}^{N}\sum_{t=-N}^{N}(N_1C_{1s}C_{1t} + QC_{2s}C_{2t})C_{1(r-s-t)} - \frac{8\lambda}{3}C_{2r} = \frac{8}{j\pi^2}[1-(-1)^j]p_{sr}$$

$$r = 0,1,2 \ldots N \quad (17)$$

$$[-r^2\omega^2 + \kappa ir\omega + M_2]C_{2r} + \sum_{s=-N}^{N}\sum_{t=-N}^{N}(N_2C_{2s}C_{2t} + QC_{1s}C_{1t})C_{2(r-s-t)} + \frac{8\lambda}{3}C_{1r} = 0 \qquad r = 0,1,2, \ldots N \quad (18)$$

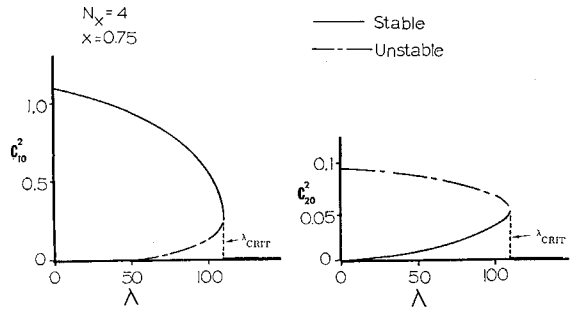

Fig. 2 Static modal deflection at panel ¾ chord vs dynamic pressure parameter.

It should be noted that

$$\omega = 0 \text{ if } r = 0 \text{ and } p_{sr} = \begin{cases} p_s \text{ if } r = 0 \\ 0 \text{ if } r \neq 0 \end{cases}$$

Here one is concerned with a steady-state oscillatory domain and the initial phase of the motion is nonessential. This means that the imaginary part of one of the harmonics of the complex modal amplitudes can be arbitrarily equated to zero. Thus only $4N + 2$ real constants need be determined from Eqs. (17) and (18).

Static Deflection

The static deflections are determined from Eqs. (17) and (18) with the time dependent modal amplitudes equated to zero. This yields a set of nonlinear algebraic equations studied by Fralich[3]:

$$(M_1 + N_1C_{10}^2 + QC_{20}^2)C_{10} - (8\lambda/3)C_{20} = (8/j\pi^2)[1-(-1)^j]p_s \quad (19)$$

$$(M_2 + N_2C_{20}^2 + QC_{10}^2)C_{20} + (8\lambda/3)C_{10} = 0 \quad (20)$$

The static configurations of the panel in the presence of an airstream are found from Eqs. (19) and (20) for various values of the static pressure parameter p_s, and the dynamic pressure parameter λ. A typical case was considered and the results are shown in Fig. 2. The effect of the aerodynamic forces on the static deflection is evident from this figure. When λ is zero the aerodynamic forces acting on the plate vanish and the stable static configuration is determined. As λ is increased, the aerodynamic forces increase which tend to decrease the static deflection of the plate. This decrease of plate deflection is continued and at λ_{CRIT} the aerodynamic forces cause a sudden flattening of the panel which, for any increase in λ, represents the stable static configuration about which the flutter motion will be observed.

Limit-Cycle Oscillation

The only stable static configuration of the plate occurring at values of λ greater than λ_{CRIT} is the flat plate. Thus for the flutter motion, the zero harmonic of each of the Fourier series representing the modal amplitudes is zero. This is used in rewriting Eqs. (17) and (18) to obtain equations from which the harmonics of the modal amplitudes for a limit-cycle oscillation can be obtained

$$[-r^2\omega^2 + \kappa ir\omega + M_1]C_{1r} + \sum_{s=1}^{N}\sum_{t=1}^{N}[(N_1C_{1s}{}^*C_{1t}{}^* + QC_{2s}{}^*C_{2t}{}^*)C_{1(r+s+t)} + 2(N_1C_{1s}{}^*C_{1t} + QC_{2s}{}^*C_{2t})C_{1(r+s-t)} + (N_1C_{1s}C_{1t} + QC_{2s}C_{2t})C_{1(r-s-t)}] - \frac{8\lambda}{3}C_{2r} = 0 \quad (21)$$

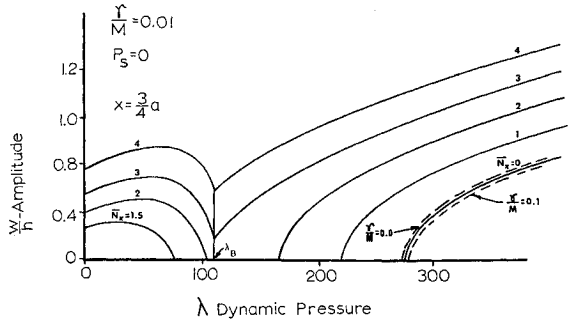

Fig. 3 Panel limit cycle amplitudes at ¾ chord point vs dynamic pressure parameter for various values of compressive end load.

$$[-r^2\omega^2 + \kappa ir\omega + M_2]C_{2r} + \sum_{s=1}^{N}\sum_{t=1}^{N}[(N_2C_{2s}{}^*C_{2t}{}^* + QC_{1s}{}^*C_{1t}{}^*)C_{2(r+s+t)} + 2(N_2C_{2s}{}^*C_{2t} + QC_{1s}{}^*C_{1t})C_{2(r+s-t)} + (N_2C_{2s}C_{2t} + QC_{1s}C_{1t})C_{2(r-s-t)} + \frac{8\lambda}{3}C_{1r} = 0 \quad (22)$$

Since flutter experiments have shown the motion of the plate to be approximately sinusoidal it is only necessary to use very few terms from the Fourier series to represent the limit-cycle oscillation. Equations (21) and (22) were solved for the modal harmonics when N was selected to be three. Modal harmonics greater than three were neglected and a parameter study of the effects of aerodynamic damping, applied midplane loads and dynamic pressure on the modal harmonics C_{nr} and frequency of oscillation ω was conducted. A plate with stiffness and geometric properties typical of those found in aerospace applications was selected and the calculations were performed to obtain information about the limit-cycle motion. The results of these calculations are shown in Fig. 3 and are representative of most of the cases considered during this investigation.

Various points within the "limit cycle oscillation" region of the linear stability diagram, Fig. 4, were investigated using one, two and three harmonics. It was found that one harmonic gave an accurate representation of the modal amplitudes over the limit cycle oscillation region with the exception of a region designated as "periodic but not simple harmonic." Outside of this "not simple harmonic" region, the error incurred in representing C_1 and C_2 by neglecting harmonics beyond the first was calculated to be less than 1%. Thus to a very good approximation the modal amplitudes of the limit cycle oscillation can be expressed as

$$C_1(t) = A\cos(\omega_L t + \epsilon_L) \quad (23)$$

$$C_2(t) = B\cos(\omega_L t) \quad (24)$$

where A, B, ω_L, ϵ_L can be calculated from Eqs. (21) and (22).

Stability of Limit Cycle

Within the "periodic but not simple harmonic" region there is some disagreement between the limit cycle prediced by the method outlined above and that given by Dowell.[4] A stability study of the predicted steady state limit cycle was accomplished to investigate the above disagreement. Each modal amplitude of the previously determined limit-cycle amplitude is perturbed by a small amount

$$C_n(t) = C_{nL}(t) + C_{np}(t) \qquad n = 1,2 \quad (25)$$

where C_{nL} is the modal amplitude of the limit-cycle oscillation determined from Eqs. (23) and (24). C_{np} is the small perturbation and satisfies $C_{np} \ll C_{nL}$.

The relations given by Eq. (25) are substituted into Eqs. (13) and (14). The approximate solutions given by Eqs. (23) and (24) are assumed to satisfy Eqs. (21) and (22) exactly, and only linear terms in the perturbation amplitudes are retained to study small oscillations about the limit cycle. This produces a coupled set of differential equations of the Mathieu type

$$\frac{d^2C_{1P}}{dt^2} + \kappa\frac{dC_{1P}}{dt} + \left\{M_1 + \frac{3N_1A^2}{2}[1 + \cos2\omega_L t - 2\epsilon_L\sin\omega_L t] + \frac{QB^2}{2}[1 + \cos2\omega_L t]\right\}C_{1P} + \left\{\frac{QAB}{2}[1 + \cos2\omega_L t - \epsilon_L\sin2\omega_L t] - \frac{8\lambda}{3}\right\}C_{2P} = 0 \quad (26)$$

$$\frac{d^2C_{2P}}{dt^2} + \frac{dC_{2P}}{dt} + \left\{M_2 + \frac{3N_2A^2}{2}[1 + \cos2\omega_L t] + \frac{QA^2}{2}[1 + \cos2\omega_L t - 2\epsilon_L\sin\omega_L t]\right\}C_{2P} + \left\{\frac{QAB}{2}[1 + \cos2\omega_L t - \epsilon_L\sin2\omega_L t] + \frac{8\lambda}{3}\right\}C_{1P} = 0 \quad (27)$$

These equations are integrated numerically to obtain the time history of the modal amplitudes of the perturbed motion. The stability of the limit-cycle oscillation can then be determined. If the amplitude of the perturbed oscillation returns to zero or a constant small magnitude, then the limit-cycle oscillation is stable. If the amplitude of the perturbed oscillation becomes unbounded then the limit-cycle oscillation is unstable. Two points from the limit cycle oscillation region of Fig. 4 were selected for stability study as being representative of all points in that region. Time histories of the perturbed motion about the limit-cycle oscillation for these two points are presented in Figs. 5 and 6. Figure 5 presents a case where the limit-cycle is stable and Fig. 6 depicts a case where the limit cycle is unstable. The case shown in Fig. 6 is representative of the unstable limit-cycles occurring within the not simple harmonic region of Fig. 4.

If the motion about the limit cycle is unstable, the steady state limit cycle predicted by Eqs. (23) and (24) will not exist. It was assumed, a priori, that a steady-state limit cycle could be obtained; but within the not simple harmonic region, this assumption is false. Therefore, a time history of the oscillation including all transient motion is required to study the actual motion within this region.

It is speculated that the plate motion within this questionable region can be explained by the following. The plate selects first a static configuration about which a limit cycle motion occurs; but as time progresses, small disturbances within the system cause the panel to jump to a new static configuration about which a new limit cycle motion occurs. This means that there exist at least two static configurations, with equal strain energy levels, which the plate selects with a given period. A possible cause of the plate jumping from one static configuration to another is the nonlinear behavior of the interaction of the buckling and flutter phenomena neglected here.

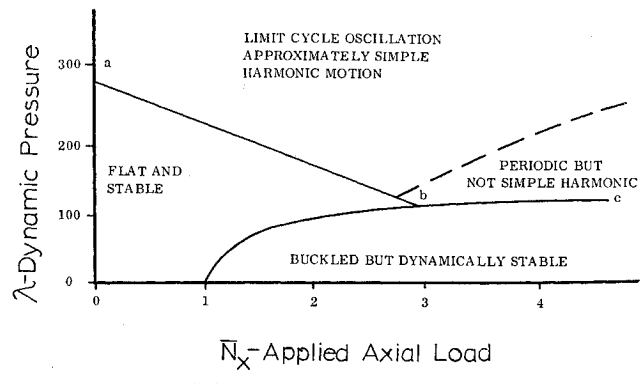

Fig. 4 Classical flutter and buckling stability diagram.

IV. Plate Response to Random Pressure Loading

An oscillating plate in an airstream is usually subjected to random pressure loads from the turbulent boundary layer causing a random forced response of the plate. The random pressure loading neglected in Eqs. (17) and (18) will now be included to determine this additional response. Following McClure[5] and Fung,[6] we represent the aerodynamic pressure as

$$p(x,y,w,t) = p_D(w,t) + p_{DB}(x,y,w,t) + p_R(x,y,t) \quad (28)$$

where p_D is the incremental aerodynamic pressure induced by the panel deformation without boundary layer effects, p_{DB} is the boundary layer effect on the pressure induced by panel deformation, and p_R is the random pressure representing the random fluctuations of the turbulent boundary layer. Here p_R is distributed both spatially and temporally to represent the random fluctuations of turbulence. The pressure correlation functions are adapted from those given by Tack and Lambert.[7]

$$\langle p(x,t)p(x^1,t^1)\rangle = \pi L_x\langle p^2\rangle g(L_y,ly)\delta(x - x^1 - v\tau)e_{-|\tau|/\delta} \quad (29)$$

where the symbols are defined in Ref. 7. Since Eq. (29) is a phenomenological pressure field, it will be assumed that the plate deformation has no effect upon the form of the pressure correlation function, but the experimental constants should be determined from flexible plate measurements. Here, p_{DB} will be neglected because of the following:

1) McClure[5] has shown the effect of the boundary layer on the stability boundary of a plate is only critical at low supersonic Mach numbers, and the effect of the boundary layer vanished as the Mach number approached and exceeded $(2)^{1/2}$. The present study is not applicable at this low supersonic Mach number unless an aerodynamic theory other than piston theory is selected and the boundary effect included in the manner of Olson.[8]

2) Olson[8] has shown for a finite plate undergoing only streamwise bending, that piston theory is an approximate representation of boundary-layer results at freestream Mach numbers greater than two. In this section, a flat plate undergoing streamwise bending only will be selected as the structural model used to determine the random response of a panel with turbulent boundary layer.

Because of the preceding arguments, p_{DB} was neglected, p_D was given by piston theory, and p_R was given by Eq. (29). This means that the pressure fluctuations can be separated into those due to panel deformation and those due to the turbulent boundary layer.

Supercritical Response

The supercritical response is the panel response after the onset of the flutter motion. An investigation of the panel response occurring before the onset of the flutter motion is contained in Ref. 9. The panel motion is considered to be composed of a previously determined flutter motion and a small random response about the flutter motion. The modal amplitudes can be represented as

$$C_n = C_{nL} + C_{nR} \text{ where } C_{nR} \ll C_{nL} \qquad n = 1,2 \quad (30)$$

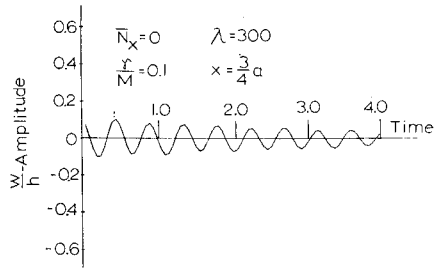

Fig. 5 Time history of the perturbed motion about a stable limit cycle.

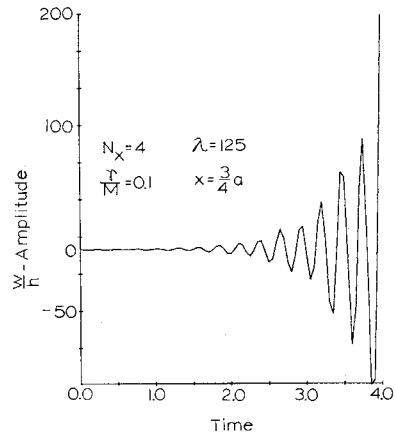

Fig. 6 Time history of the perturbed motion about an unstable limit cycle.

where C_{nL} are the modal amplitudes of the limit cycle oscillation determined previously from Eqs. (23) and (24) and C_{nR} are the modal amplitudes of the random response.

The equations governing panel motion in the supercritical region, with effects of the turbulent boundary layer, are obtained from Eqs. (13) and (14) with p_s zero and p_{1R} and p_{2R} nonzero. Relations (30) are used to reduce Eqs. (13) and (14) (after linearizing with respect to C_{nR}) to a coupled set of linear nonhomogeneous differential equations for the modal random response

$$\frac{d^2C_{1R}}{d\tau^2} + \kappa\frac{dC_{1R}}{d\tau} + [M_1 + 3N_1C_{1L}^2 + QC_{2L}^2]C_{1R} + \left[QC_{2L}C_{1L} - \frac{8\lambda}{3}\right]C_{2R} = p_{1R} \quad (31)$$

$$\frac{d^2C_{2R}}{d\tau^2} + \kappa\frac{dC_{2R}}{d\tau} + [M_2 + 3N_2C_{2L}^2 + QC_{1L}^2]C_{2R} + \left[QC_{2L}C_{1L} + \frac{8\lambda}{3}\right]C_{1R} = p_{2R} \quad (32)$$

It is desired to determine the modal mean-square responses about a previously defined flutter motion. The previous sections indicate that the limit-cycle oscillation is approximately sinusodial and given by Eqs. (23) and (24). The expression previously determined for the limit-cycle oscillation is substituted into Eqs. (31) and (32) yielding the following panel random response equations:

$$\frac{d^2C_{1R}}{d\tau^2} + \kappa\frac{dC_{1R}}{d\tau} + [P_1 + p_1\cos 2\omega_L\tau]C_{1R} + [R_1 + r_1\cos 2\omega_L\tau]C_{2R} = p_{1R} \quad (33)$$

$$\frac{d_2C_{2R}}{d\tau^2} + \kappa\frac{dC_{2R}}{d\tau} + [P_2 + p_2\cos 2\omega_L\tau]C_{2R} + [R_2 + r_2\cos 2\omega_L\tau]C_{1R} = p_{2R} \quad (34)$$

This is a coupled set of nonhomogeneous differential equations of the Mathieu type.

Equations (33) and (34) are transformed by the following Fourier transformation:

$$C_{nR}(\bar{\gamma}) = \int_{-\infty}^{\infty} C_{nR}(\tau)e^{-i\bar{\gamma}\tau}d\tau \qquad n = 1,2 \quad (35)$$

The transformed equations for the modal amplitudes are

$$[-\bar{\gamma}^2 + i\kappa\bar{\gamma} + p_k]C_{kR} + (p_k/2)[C_{kR}(\bar{\gamma} - 2\omega_L)] + R_mC_{mR} + (r_m/2)[C_{mR}(\bar{\gamma} - 2\omega_L) + C_{mR}(\bar{\gamma} + 2\omega_L)] = p_{kR}(\bar{\gamma}) \; k,m = 1,2 \; k \neq m \quad (36)$$

The relation

$$\bar{\gamma} = \gamma_0 \pm 2n\omega_L \; n = 0,1,2, \ldots, \infty \; 0 \leq \gamma_0 < 2\omega_L \quad (37)$$

is substituted into Eqs. (36) and one obtains the system of

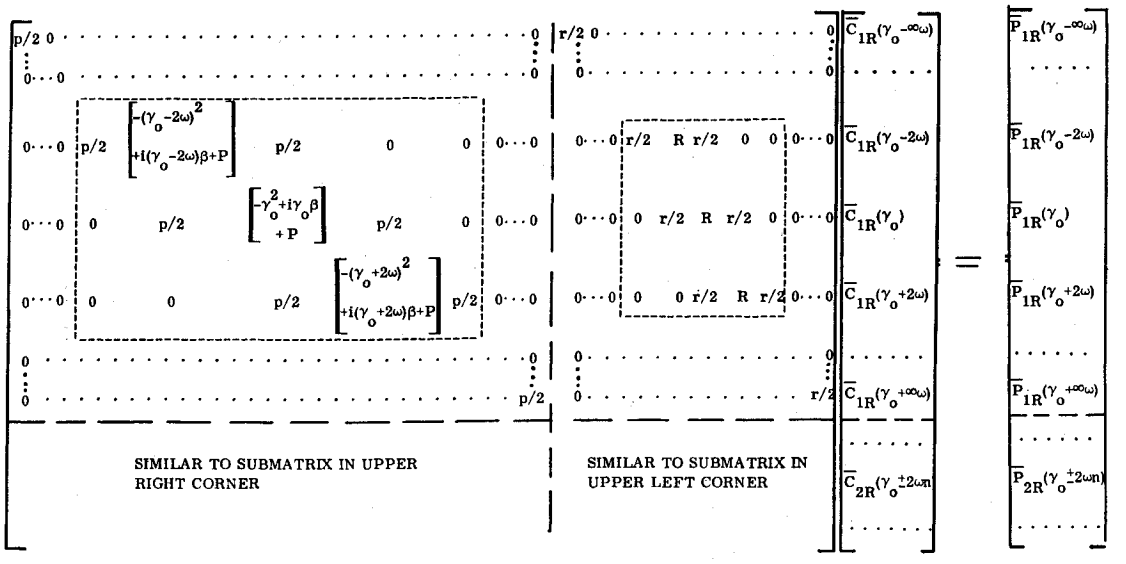

(38)

linear algebraic equations shown in the matrix equation (38). Equation (38) represents an infinite set of linear algebraic equations, from which the modal amplitudes C_{1R} and C_{2R} can be determined for particular transformed forcing functions $p_{nR}(\bar{\gamma})$. This infinite matrix equation must be reduced to finite size before solutions can be obtained. Equation (38) will yield approximate solutions if it is assumed that the transformed modal response, $C_{nR}(\bar{\gamma})$, is zero when $\bar{\gamma} \geq 2N\omega_F$. The validity of this assumption is enforced by specifying N large enough so that the contribution of $C_{nR}(\gamma)$, when $\bar{\gamma} \geq 2N\omega_F$, is negligible. The matrix size of Eq. (38) can thus be reduced to a finite number and solutions of this resulting finite matrix equation can be calculated, at particular values of $\bar{\gamma}$. The entire range of $\bar{\gamma}$ may be specified from Eq. (37) by varying γ_0 between zero and $2\omega_F$. The approximate finite matrix equation obtained from Eq. (38) is inverted and the modal response curve, to a known forcing function, calculated over all values of $\bar{\gamma}$.

Two example problems, demonstrating the above method, are described in Ref. 9 for deterministic forcing functions p_{kR}. However, for the problem considered herein (i.e., effect of the boundary layer), the forcing function is known only in a probabilistic sense so further analysis is necessary. The matrix Eq. (38) is symbolically

$$\begin{bmatrix} \\ A(\gamma_0;2\omega) \\ \\ \end{bmatrix} \begin{bmatrix} C(\gamma_0 - 2N\omega) \\ \cdots \\ C(\gamma_0) \\ \cdots \\ C(\gamma_0 + 2N\omega) \end{bmatrix} = \begin{bmatrix} P(\gamma_0 - 2n\omega) \\ \cdots \\ P(\gamma_0) \\ \cdots \\ P(\gamma_0 + 2N\omega) \end{bmatrix} \tag{39}$$

Now positive γ_0 can be replaced by negative γ_0, the matrix $[A(-\gamma_0)]$ rearranged to form $[B(-\gamma_0)]$ and the resulting matrix equation inverted to determine the response

$$\begin{bmatrix} C(-\gamma_0 + 2N\omega) \\ \cdots \\ C(-\gamma_0) \\ \cdots \\ C(-\gamma_0 - 2N\omega) \end{bmatrix} = \begin{bmatrix} \\ B(-\gamma_0;2\omega) \\ \\ \end{bmatrix}^{-1} \begin{bmatrix} P(-\gamma_0 + 2N\omega) \\ \cdots \\ P(-\gamma_0) \\ \cdots \\ p(-\gamma_0 - 2N\omega) \end{bmatrix} \tag{40}$$

The spectral density of the cross correlation of the response is calculated from

$$[S_c(\gamma_0;2\omega)] = [A(\gamma_0;2\omega)]^{-1}[S_p(\gamma_0;2\omega)][B(-\gamma_0;2\omega)]^{-1^T} \tag{41}$$

where $[S_p(\gamma_0;2\omega)]$ is determined from the known distribution of pressure for the turbulent boundary layer. This cross correlation function for modal response allows one to determine the mean squared modal response as

$$\langle C^2 \rangle = \frac{1}{2}\int_{-\infty}^{\infty} S_c(\omega)d\omega \tag{42}$$

V Nonlinear Aerodynamic Loading

Consider now an isotropic, thin, two-dimensional panel, or plate column. This system can be viewed as the two-dimensional counterpart of the system illustrated in Fig. 1, but with infinite panel span. In addition, there is an in-plane restraint spring at the edge $X = a$ with spring constant K per unit length along the span. Hamilton's principle, as stated in Eq. (7), will be used to derive the equations of motion.

The transverse kinetic energy of the panel is given by

$$T = \frac{\rho h}{2}\int_0^a \left(\frac{\partial w}{\partial t}\right)^2 dx \tag{43}$$

The potential energy reads

$$U + V = \frac{1}{2}\int_0^a \left\{\frac{Eh}{1-\nu^2}\left[\frac{\partial u}{\partial x} + \frac{1}{2}\left(\frac{\partial w}{\partial x}\right)^2\right]^2 + D\left(\frac{\partial^2 w}{\partial x^2}\right)^2\right\} dx + \bar{N}_x h(B_0 + B_R) + \frac{1}{2}Kh^2B_0^2 \tag{44}$$

B_R will respent the end displacement resulting when N_x is applied, and B_0 will represent the subsequent in-plane end displacement.

The panel displacements u and w are approximated by the following modal series:

$$u(x,t) = h[B_R + B_0(t)]\frac{x}{a} + \sum_{m=1}^{2N} hB_m(t)\sin m\alpha x \tag{45}$$

$$w(x,t) = \sum_{m=1}^{N} hC_m(t)\sin m\alpha x \tag{46}$$

The virtual work of the applied aerodynamic loads

$$(\delta W_e)_m = \int_0^a Ah\sin m\alpha x \delta C_m dx, \quad m = 1,2,\ldots N \tag{47}$$

Here the aerodynamic loading A is approximated by the linear piston-theory terms from Eq. (3) plus two additional second-order piston-theory terms

$$A = \frac{2q}{M}\left\{\frac{\partial w}{\partial x} + \frac{1}{U_\infty}\frac{\partial w}{\partial t} + \frac{(\gamma_a + 1)M}{4}\left[\left(\frac{\partial w}{\partial x}\right)^2 + \frac{2}{U_\infty}\frac{\partial w}{\partial x}\frac{\partial w}{\partial t}\right]\right\} \tag{48}$$

The two nonlinear terms in this expression have been found to be the ones most important for parameter ranges anywhere near those found in practice. Since hypersonic speeds are of interest here, $M \gg 1$, some coefficients have also been simplified by making use of this assumption.

Equations (45) and (46) are used to substitute for u and w in the expressions for potential energy, and virtual work. Application of Hamilton's principle, Eq. (7), then produces the equations of motion. The variation with respect to B_R (assuming all $C_m = 0$) gives

$$-\bar{N}_x - [Eh^2/a(1-\nu^2)]B_R = 0 \tag{49}$$

while the variation with respect to B_0 yields

$$-\bar{N}_x - KhB_0 - \frac{Eh^2(B_R + B_0)}{a(1-\nu^2)} - \frac{\pi^2 Eh^3}{4a^2(1-\nu^2)} \sum_{m=1}^{N} m^2 C_m{}^2 = 0 \tag{50}$$

The final in-plane equilibrium equation is obtained from the coefficient of

$$\frac{Eh}{1-\nu^2}\left[\frac{\pi^2 m^2 h}{2a} B_m + \frac{m\pi^3 h^2}{8a^2}\left(\sum_{\substack{i=1\\ i+j=m}}^{N}\sum_{j=1}^{N} ijC_iC_j + 2\sum_{\substack{i=1\\ i-j=m}}^{N}\sum_{j=1}^{N} ijC_iC_j\right)\right] = 0 \tag{51}$$

A considerably more complicated transverse equilibrium equation, resulting from varying with respect to the C_m, completes the set. Equations (49–51) are then used to eliminate all of the modal amplitudes except the C_m in this equation. After cancellation of terms and rearrangement in terms of dimensionless variables and parameters, this equation becomes

$$\frac{1}{2}\frac{d^2C_m}{d\tau^2} + \frac{1}{2}m^2(m^2 - N_x)C_m + \frac{3}{2}m^2\alpha' C_m \sum_{i=1}^{N} i^2 C_i{}^2 + \lambda \sum_{i=1}^{N} \frac{mi[1-(-1)^{m+i}]}{i^2 - m^2} C_i + \frac{1}{2}\kappa\frac{dC_m}{d\tau} + \frac{(\gamma_a+1)\pi m}{4}\lambda_m \frac{h}{a}\sum_{i=1}^{N}\sum_{j=1}^{N} \frac{ij(m^2 - i^2 - j^2)[1-(-1)^{m+i+j}]}{[m^2-(i-j)^2][m^2-(i+j)^2]} \times C_iC_j + \frac{(\gamma_a+1)\pi}{8}\kappa M\frac{h}{a}\left[\sum_{\substack{i=1\\ i+j=m}}^{N}\sum_{j=1}^{N} iC_i\frac{dC_j}{d\tau} + \sum_{\substack{i=1\\ i-j=m}}^{N}\sum_{j=1}^{N}\left(jC_j\frac{dC_i}{d\tau} - iC_i\frac{dC_j}{d\tau}\right)\right] = 0$$

$$m = 1,2,\cdots,N \tag{52}$$

With initial C_m and their first derivatives specified, these equations can be integrated numerically by computer to produce the panel motion versus time. The piston-theory aerodynamic terms permit this, since they are valid for transient motion. This approach follows that of Dowell,[4] who derived similar equations, but did not consider nonlinear aerodynamic loading.

The number of independent parameters in Eqs. (52) can be further reduced by use of a transformation proposed by Dowell[4]

$$C_m(\tau) = (a')^{-1/2}\tilde{C}_m(\tau) \tag{53}$$

Rewriting Eqs. (52) in terms of the $\tilde{C}_m$ produces equations where the in-plane restraint parameter α' appears only with Mh/a in the combination $Mh/a(\alpha')^{1/2}$. This new parameter can be viewed as a measure of the relative importance of the nonlinear aerodynamic terms in the equations of motion.

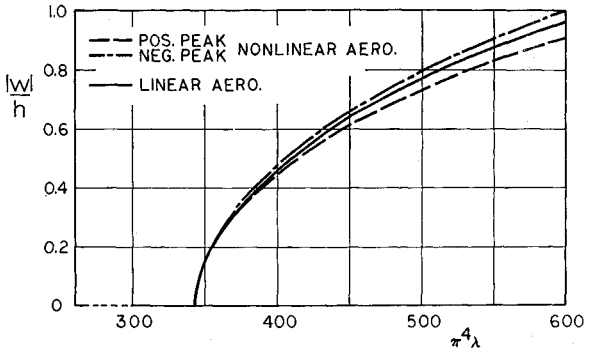

Fig. 7 Maximum absolute value of W/h at $x/a = \frac{3}{4}$ vs dynamic-pressure parameter λ.

There are two nonlinear mechanisms at work: one, the nonlinear interaction between in-plane panel stresses and transverse deformation, which provides a stabilizing influence on the panel motion in that it acts to restrain further deformation; the other, the nonlinear aerodynamic loading, which is destablizing in that it acts to increase any deformation. It is the interplay between these two mechanisms that distinguishes panel flutter at hypersonic speeds from that at supersonic speeds. However, it is emphasized that the addition of higher-order aerodynamic nonlinearities will, in general, prevent combining α' and Mh/a into a single parameter.

Hence the panel motion can be represented as follows:

$$w(x,t) = [h/(\alpha')^{1/2}]F_n[x/a,\tau;\ \mathbf{C}_0,N_x,\lambda,\lambda_a,\gamma_a,\gamma/M,\ Mh/a(\alpha')^{1/2}] \tag{54}$$

Here $\mathbf{C}_0$ represents the initial state-space vector, whose $2N$ components are the initial values of the modal amplitudes and their derivatives with respect to τ. This vector will not always govern the asymptotic behavior of w; an instance where this does occur will be discussed below.

Effect of Aerodynamic Nonlinearities on Postcritical Response

Suppose now that some $\mathbf{C}_0$ is chosen, the other parameters are fixed, and Eqs. (52) are integrated to give a time history of the panel motion. If the panel is stable, the motion will subside with time; if it is unstable, the initial transient will be followed by a stable limit cycle (exceptions to this have been discussed previously). Let us first consider values of λ and N_x that place the panel on the unstable side of the linear stability boundary. In this case, the amplitude, frequency, and form of the limit cycle are independent of $\mathbf{C}_0$. Such a limit cycle would also be observed if the nonlinear aerodynamic terms were left out, but it would be expected to be different. These differences are illustrated in Fig. 7, which plots the maxima of the limit cycle at $x = 0.75a$ vs λ. Other parameters used are $N_x = 0$, $\gamma/M = 0.01$, $Mh/a = 0.05$, $\alpha' = 1.0$, and $N = 6$. With linear aerodynamic loading, the panel moves as far into the flow as it does into the cavity; with nonlinear aerodynamic loading, the peak into the flow ($+w$) is reduced, while the peak into the cavity ($-w$) is increased in magnitude. The limit-cycle frequency is unaffected by the nonlinear aerodynamic loading. Hence the primary effect is to introduce a bias to the panel motion into the cavity. This bias comes from the nonlinear aerodynamic term proportional to $(\partial w/\partial x)^2$, which produces an overpressure, tending to push the panel into the cavity, for any excursion of the panel from its flat undisturbed state. The effect of reducing the in-plane restraint is depicted in Fig. 8, which plots the same maxima in Fig. 7 vs α' for $\lambda = 550$. The other parameters are the same as used for Fig. 7. The aforementioned bias to the panel motion is seen to increase with decreasing α', but the overall changes are not severe. Furthermore, the panel stresses, which are of primary interest,

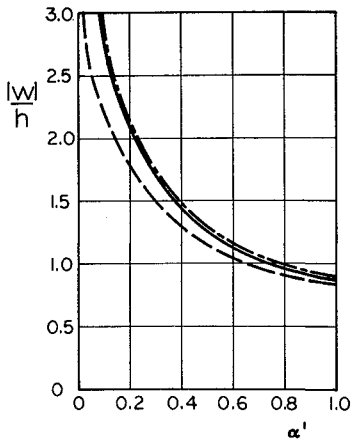

Fig. 8 Maximum absolute value of W/h at $x/a = \frac{3}{4}$ vs in-plane restraint parameter α' for $\lambda = 550$. Curve legend same as in Fig. 7.

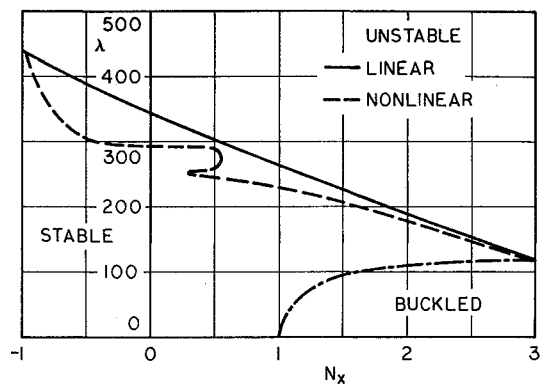

Fig. 9 Comparison of linear and nonlinear stability boundaries.

are affected even less. Stress distributions in the panel were calculated at various instants in the time histories; the maximum stresses with nonlinear aerodynamic loading were at most 5% greater than those calculated from the corresponding time histories with linear aerodynamic loading.

Effect of Aerodynamic Nonlinearities on Stability

It is known from studies of simpler systems with nonlinear nonconservative applied loads[10] that the stability of such systems is governed also by the initial conditions. That is, a system can be stable for small initial disturbances, but unstable for larger ones. For the panel, this means that amplitude-sensitive regions of instability can be found in a parameter domain that would be stable one on the basis of a theory with linear aerodynamic loading. It would be a formidable, if not impossible, task to exhibit analytically the dependence of this region on $\mathbf{C}_0$, which for $N = 6$ has 12 components. Reference 10 suggests a simplification of this problem by calculating a total energy of the system such that any combination of the components of $\mathbf{C}_0$ producing a greater energy will result in unstable motion. For a first step, it was decided to examine the stability of the panel to an initial disturbance of fixed total energy E_0, with the contribution to E_0 from each component of C_0 also specified.

Equation (44) for the total energy was rewritten in terms of the modal amplitudes. The in-plane equilibrium equations were used to eliminate the in-plane modal amplitudes in favor of the C_m, and the resultant expression, in dimensionless form, reads

$$E_0 = (U + V)/Dh^2\pi\alpha^3 = 1/4 \sum_{m=1}^{N} \left(\frac{dc_m}{d\tau}\right)^2 + 3/8\alpha' \sum_{m=1}^{N} \sum_{n=1}^{N} m^2n^2C_m{}^2C_n{}^2 + 1/4 \sum_{m=1}^{N} m^2(m^2 - N_x)C_m{}^2 \tag{55}$$

A value for E_0 of $1750\pi^4$ was chosen; this energy level is roughly comparable to the energy levels in the panel during flutter motion near but on the unstable side of the linear stability boundary. It was further decided, purely arbitrarily, to set all the components of $\mathbf{C}_0$ equal to zero except for $C_1(0) = -C_2(0)$. A stability boundary for initial conditions given in this manner is plotted in Fig. 9 and compared with the linear stability boundary. Other parameters are $N = 6$, $\gamma/M = 0.01$, $Mh/a(\alpha')^{1/2} = 0.158$ (say, $Mh/a = 0.05$, $\alpha' = 0.1$). This stability boundary was obtained by fixing λ and N_x and integrating Eqs. (52) with initial conditions calculated as just described.

VI. Concluding Remarks

The Rayleigh-Ritz approximation to Hamilton's variational principle was used to reduce von Karman's large deflection Eqs. (1) and (2) to a coupled set of ordinary differential Eqs. (13) and (14). The Rayleigh-Ritz approximation assumes satisfaction of only the plate geometric boundary conditions while the Galerkin approximation assumes satisfaction of both geometric and forced boundary conditions. Thus, use of the Rayleigh-Ritz method will allow consideration of plate flutter problems with all the complex boundary conditions encountered in actual practice. Equations (13) and (14) were then reduced to a set of nonlinear algebraic Eqs. (17) and (18) with the Galerkin method applied over the temporal variable. If this method is used, then an unsteady aerodynamic theory based on the assumption of simple harmonic motion may be selected to represent the aerodynamic pressure. The aerodynamic theories of simple harmonic motion are well developed while those of non-simple harmonic motion are nonexistent or, at best, expressed in a numerical form. The above methods have been used with the analysis of a thin circular cylindrical shell as described in Ref. 9.

In connection with the hypersonic panel-flutter problem, it is evident that accurately representing the degree of in-plane restraint is the key to determining whether or not amplitude sensitive instability will be of practical importance. Clearly, Mh/a is not likely to be anywhere close to unity, so the value of α' must be smaller than unity in order for nonlinear aerodynamic terms to have an effect. (The value of α' ranges from unity, for $K = \infty$, to zero, for $K = 0$). At the present time, parametric studies are in progress, in order to determine changes in the nonlinear boundary of Fig. 9 due to variations in γ/M, $Mh/a(\alpha)^{1/2}$, E_0, and the model content of E_0.

References

[1] Bolotin, V. V., *Nonconservative Problems of the Theory of Elastic Stability*, MacMillan, New York, 1963, pp. 257–306.

[2] Küssner, H. G., "On the Nonlinear Approach to the Aeroelastic Stability Theory," Rept. 246, April 1959, AGARD.

[3] Fralich, R. W., "Postbuckling Effects on the Flutter of Simply Supported Rectangular Panels at Supersonic Speeds," TN D-1615, March 1963, NASA.

[4] Dowell, E. H., "Nonlinear Oscillation of a Fluttering Plate," *AIAA Journal*, Vol. 4, No. 7, July 1966, p. 1267.

[5] McClure, J. D., "On Perturbed Boundary Layer Flows," Rept. 62-2, June 1962, MIT Fluid Dynamics Research Lab.

[6] Fung, Y. C., "Some Recent Contributions to Panel Flutter," *AIAA Journal*, Vol. 1, No. 7, Jan. 1963, pp. 898–909.

[7] Tack, D. H. and Lambert, R. F., "Response of Bars and Plates to Boundary-Layer Turbulence," *Journal of the Aeronautical Sciences*, Vol. 29, No. 3, March 1962, p. 311.

[8] Olson, M. D., "On Comparing Theory and Experiment for the Supersonic Flutter of Circular Cylindrical Shells," AFOSR 66-0944, June 1966, California Institute of Technology.

[9] Eastep, F. E., "Nonlinear Oscillations of Elastic Panels in a Supersonic Nonviscous Airstream," SUDAAR 354, Aug 1968, Dept. of Aeronautics and Astronautics, Stanford Univ., Calif.

[10] Dimantha, P. C. and Roorda, J., "On the Domain of Asymptotic Stability of Nonlinear Nonconservative Systems," *Applied Scientific Research*, Vol. 20, March 1969, pp. 272–288.